24 Applications of Quantum Information in the Density-Matrix Renormalization Group

Ö. Legeza[1], R.M. Noack[2], J. Sólyom[1], and L. Tincani[2]

[1] Research Institute for Solid State Physics and Optics, H-1525 Budapest, Hungary
[2] Fachbereich Physik, Philipps-Universität Marburg, 35032 Marburg, Germany

In the past few years, there has been an increasingly active exchange of ideas and methods between the formerly rather disjunct fields of quantum information and many-body physics. This has been due, on the one hand, to the growing sophistication of methods and the increasing complexity of problems treated in quantum information theory, and, on the other, to the recognition that a number of central issues in many-body quantum systems can fruitfully be approached from the quantum information point of view. Nowhere has this been more evident than in the context of the family of numerical methods that go under the rubric density-matrix renormalization group. In particular, the concept of entanglement and its definition, measurement, and manipulation lies at the heart of much of quantum information theory [1]. The density-matrix renormalization group (DMRG) methods use properties of the entanglement of a bipartite system to build up an accurate approximation to particular many-body wave functions. The cross-fertilization between the two fields has led to improvements in the understanding of interacting quantum systems in general and the DMRG method in particular, has led to new algorithms related to and generalizing the DMRG, and has opened up the possibility of studying many new physical problems, ones of interest both for quantum information theory and for understanding the behavior of strongly correlated quantum systems [2].

In this line, we discuss some relevant concepts in quantum information theory, including the relation between the DMRG and data compression and entanglement. As an application, we will use the quantum information entropy calculated with the DMRG to study quantum phase transitions, in particular in the bilinear-biquadratic spin-one chain and in the frustrated spin-1/2 Heisenberg chain.

24.1 Basic Concepts of Quantum Information Theory

Perhaps the most fundamental measure in quantum information is the von Neumann entropy, which quantifies the quantum information or entanglement between two parts of a bipartite system. For a system of size N, it is defined as

$$s(N) = -\mathrm{Tr}\left[\rho^{(N)} \ln \rho^{(N)}\right] . \tag{24.1}$$

Here $\rho^{(N)}$ is the density matrix for the system and the trace is over the degrees of freedom of the system. Implicit in this description is that the system can be thought

Ö. Legeza et al.: *Applications of Quantum Information in the Density-Matrix Renormalization Group*, Lect. Notes Phys. **739**, 653–664 (2008)
DOI 10.1007/978-3-540-74686-7_24

of as forming one part of a larger, bipartite system which can always be constructed to be in a pure state.

The von Neumann entropy has been found to be intimately connected to many-body properties of a quantum system such as the quantum criticality. In one dimension, $s(N)$ will increase logarithmically with N if the system is quantum critical, but will saturate with N if the system is not [3, 4]. If a quantum critical system is also conformally invariant, additional, specific statements can be made about the entropy (see below) [5]. In higher dimensions, the von Neumann entropy will be bounded from below by a number proportional to the area (or length or volume, as appropriate) of the interface between the two parts of the system [6].

Since the von Neumann entropy is also a quantification of the fundamental approximation in the DMRG, a number of entanglement-based approaches to improve the performance and to extend the applicability of DMRG [2, 7, 8, 9], have been developed in the past few years [10, 11, 12, 13, 14, 15, 16].

For a more extensive discussion of the relationship of entanglement and von Neumann entropy with the fundamentals of the DMRG, see Chap. 20 of this volume, especially Sects. 2 and 6.

24.1.1 DMRG and Quantum Data Compression

The reduction of the Hilbert space carried out in the DMRG method is closely related to the problem of quantum data compression [17, 18]. In quantum data compression, the Hilbert space of the system Λ is divided into two parts: The "typical subspace" Λ_{typ}, which is retained, and the "atypical subspace" Λ_{atyp}, which is discarded. For pure states, there is a well defined relationship between Λ_{typ} and the von Neumann entropy of the corresponding ensemble. In general, it has been shown that

$$\beta \equiv \ln\left(\dim \Lambda_{\text{typ}}\right) - s \;, \tag{24.2}$$

is independent of the system size for large enough systems [11, 19].

Since one fundamentally treats a bipartite system in the DMRG, each subsystem is, in general, in a mixed state. In the context of the DMRG, the accessible information [20, 21] of mixed-state ensembles can be interpreted as the information loss due to the truncation procedure. This information loss is a better measure of the error than the discarded weight of the reduced density matrix

$$\varepsilon_{\text{TE}} = 1 - \sum_{\alpha=1}^{m} w_\alpha \;, \tag{24.3}$$

(also called the truncation error). Here the w_α are the eigenvalues of the reduced density matrix ρ of either subsystem; both must have the same nonzero eigenvalue spectrum.

Based on these considerations, the convergence of DMRG can be improved significantly by selecting the states kept using a criterion related to the accessible information. In general, the accessible information must be less than the Kholevo bound [20]

$$I \leq s(\rho) - p_{\text{typ}} s(\rho_{\text{typ}}) - (1 - p_{\text{typ}})\, s(\rho_{\text{atyp}}) \;, \tag{24.4}$$

where ρ_{typ} or ρ_{atyp} are the portions of the density matrix formed from the basis states that are kept and discarded, respectively. The probability p_{typ} is chosen to be appropriate for the corresponding binary channel. The behavior of the mutual information for particular ensembles as a function of p_{typ}, including various bounds on the mutual information can be found in [21]. For the DMRG, the atypical subspace should contain as little information as possible if the approximation is to be accurate. Assuming that this is the case, we take $p_{\text{typ}} = 1$, and the number of block states are selected so that $s(\rho) - s(\rho_{\text{typ}}) \leq \chi$. This *a priori*-defined χ satisfies a well-defined entropy sum rule which is related to the total quantum information generated by the DMRG. Deviations from this sum rule provide a measure of the error of the DMRG calculation. Therefore, χ can be chosen to control its accuracy.

Figure 24.1 shows the relative error of the ground-state energy, defined as $(E_{\text{DMRG}} - E_{\text{exact}})/E_{\text{exact}}$, plotted on a logarithmic scale for various values of the Coulomb interaction U for the one-dimensional Hubbard model. In Fig. 24.1(a), it is plotted as a function of ε_{TE}, whereas in Fig. 24.1(b), it is plotted as a function of χ. As can be seen, the error in the latter plot behaves very stably as a function of χ, even for very small values of the retained eigenvalues of ρ_{typ}. On the other hand, the error in the energy behaves somewhat less regularly as a function of ε_{TE}. Therefore, an extrapolation of the energy as a function of χ would be significantly better behaved than one as a function of ε_{TE}. We find that such behavior is representative; generically, extrapolation with χ is as stable or more stable than extrapolation with ε_{TE} for a wide variety of systems [11].

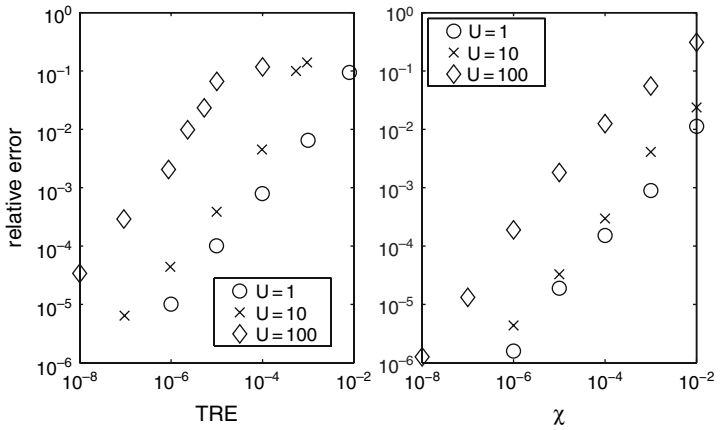

Fig. 24.1. The relative error of the ground-state energy for the half-filled Hubbard chain for various values of the on-site Coulomb interaction U on an $N = 80$-site lattice with periodic boundary conditions as a function of **(a)** the truncation error and **(b)** the threshold value of the Kholevo bound on accessible information, see (24.4). Taken from [11]

24.1.2 DMRG and Non-Local Models

Another application of quantum information to the DMRG is to non-local quantum lattice models that occur in quantum chemical applications [22] or when the Hubbard and related models are represented in momentum space [23, 24]. A general non-local fermionic Hamiltonian has the form

$$\widehat{H} = \sum_{p,q,\sigma} T^{\sigma}_{p,q}\, \widehat{c}^{\dagger}_{p,\sigma}\widehat{c}_{q,\sigma} + \sum_{p,q,r,s,\sigma,\sigma'} V^{\sigma,\sigma'}_{p,q,r,s}\, \widehat{c}^{\dagger}_{p,\sigma}\widehat{c}^{\dagger}_{q,\sigma'}\widehat{c}_{r,\sigma'}\widehat{c}_{s,\sigma}\ . \tag{24.5}$$

Here $\widehat{c}^{\dagger}_{p,\sigma}$ creates a fermion with spin σ in single-particle orbital p. In quantum chemistry, the $T^{\sigma}_{p,q}$ represent the one-particle overlap integrals, while in momentum-space models only the diagonal elements, which contain the dispersion, are nonzero. The $V^{\sigma,\sigma'}_{p,q,r,s}$ are two-particle overlap integrals, which are related to the Coulomb interaction, in quantum chemistry. For momentum-space models, $V^{\sigma,\sigma'}_{p,q,r,s}$ contains the Fourier-transformed Coulomb interaction; additional symmetries (momentum conservation, interaction only between opposite spin species, etc.) generally simplify its structure significantly.

In contrast to short-range models in real space, the optimal ordering of the "lattice sites", in such models, i.e., the orbitals of the single-particle basis, is not evident. However, finding a sufficiently good ordering seems to be crucial to formulating efficient DMRG algorithms for such systems [10, 25]. From a quantum information point of view, the lattice sites are inequivalent in general; their relative importance only becomes clear when the interaction is turned on. Therefore, the entropy profile of the bipartite partitioning of the finite system depends very much on the ordering of the lattice sites. The question, then, is how to quantify their importance in terms of quantum information. Unfortunately, there is, as yet, no clear-cut solution to this problem. However, various quantum-information-based quantities lend insight. One such quantity is the single-site entropy s^p, which is formed by taking a single site as one part of a bipartite system, and then calculating the entropy for this subsystem in the usual way. This quantity encodes the entanglement between the site and the remainder of the system, i.e., the extent to which the site shares quantum information with the rest of the system. Heuristic schemes to order sites based on this site entropy have been proposed [10]: Generally, sites with the largest single-site entropy should be placed close together in the middle of the order. For such cases the size of the typical subspace can also be reduced using entanglement-based optimization of the ordering of lattice sites [10, 11, 16, 22]. The problem, however, is that the single-site entropy does not encode the quantum information exchange between *pairs* of sites, i.e., how important it is to place particular sites in proximity to each other.

One quantity that can overcome this problem is the mutual two-site information

$$I_{p,q} \equiv \frac{1}{2}\left(s^p + s^q - s^{pq}\right)\left(1 - \delta_{pq}\right) \geq 0\ , \tag{24.6}$$

where s^{pq} is the entropy of a subsystem consisting of two (not necessarily adjacent) lattice sites p and q. This quantity has proven to be especially useful when

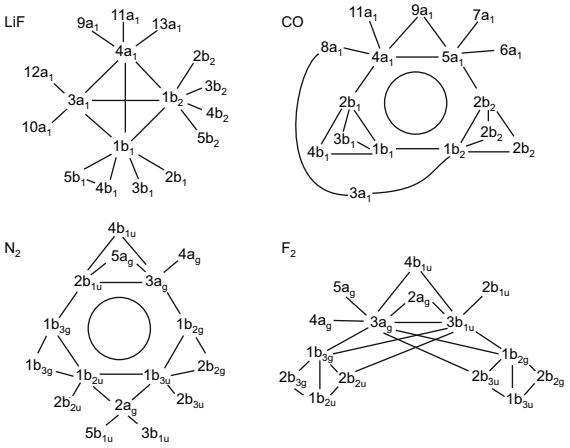

Fig. 24.2. Diagram of $I_{p,q}$ for the molecules LiF, CO, N_2, and F_2 calculated at Hartree-Fock ordering with $m = 200$: Lines connect orbital labels with $I_{p,q} > 0.01$. The circle for CO and N_2 denotes that the surrounding orbitals are all connected with each other. Taken from [22]

applied to quantum chemical systems. In Fig. 24.2, we show the topology of $I_{p,q}$ for four prototypical small molecules, LiF, CO, N_2, and F_2, with a particular basis set; for details, see [22]. As can be seen, the mutual two-site information yields a picture of the detailed connectivity of the orbitals, which is different for each molecule. An attempt to optimize ordering of orbitals using a cost function based on this information has led to moderate success [22]. However, more work needs to be done both on defining a meaningful measure of mutual two-site information, and in developing heuristics to optimize ordering based on this measure. A related problem has cropped up in an attempt to map the one-dimensional Hubbard model with periodic boundary condition to a model with open boundary conditions [16]. The transformed effective interaction, which has the form $V^{\sigma,\sigma'}_{p,q,r,s}$ (see Hamiltonian (24.5)), is then nonlocal. An analysis of the entanglement generated by these nonlocal terms has been used to optimize the site ordering. Such insights are also relevant to quantum chemical problems.

24.2 Entropic Analysis of Quantum Phase Transitions

The local measure of entanglement, the ℓ-site entropy with $\ell = 1, 2, ...N$, which is obtained from the reduced density matrix ρ, can be used to detect and locate quantum phase transitions (QPTs) [26, 27, 28, 29]. As an example, Fig. 24.3 shows the block entropy for $\ell = N/2$ for the most general isotropic spin-one chain model described by the Hamiltonian

$$H = \sum_i \left[\cos\theta \left(\boldsymbol{S}_i \cdot \boldsymbol{S}_{i+1} \right) + \sin\theta \left(\boldsymbol{S}_i \cdot \boldsymbol{S}_{i+1} \right)^2 \right] , \tag{24.7}$$

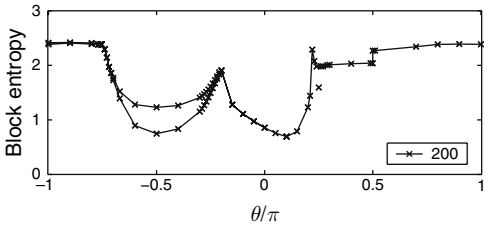

Fig. 24.3. Entropy of blocks of $\ell = N/2$ and $\ell = N/2 + 1$ sites of the bilinear-biquadratic spin $S = 1$ model for a chain with $N = 200$ sites

as a function of θ, where we take $-\pi < \theta \leq \pi$. In one dimension, the model is known to have at least four different phases [30, 31, 32]. The ground state is ferromagnetic for $\theta < -3\pi/4$ and $\theta > \pi/2$. For $-3\pi/4 < \theta < -\pi/4$, the ground state is dimerized; the point $\theta = -\pi/4$ is exactly solvable [33, 34]. In the range $-\pi/4 < \theta < \pi/4$, the system is in the Haldane phase, there is an exact solution at $\theta = \pi/4$ [35, 36, 37], and for $\pi/4 < \theta < \pi/2$, the phase is spin nematic (trimerized). The issue of whether a quantum quadrupolar phase [38, 39, 40], exists near $\theta = -3\pi/4$ has not yet been settled [41]. These phases and the corresponding QPTs are reflected in the block entropy, Fig. 24.3. The jump in the entropy at $\pi/2$ indicates a first-order transition. At $\theta = -3\pi/4$, there is only a cusp in the block entropy, but a jump in the single-entropy s^p (as defined above) indicates that this transition is first order [42]. The cusps at $\theta = -\pi/4$ and $\pi/4$ indicate second-order transitions, and the bifurcation of the entropy curves for $\ell = N/2$ and $\ell = N/2 + 1$ indicates that there is a spatially inhomogeneous dimerized phase between $-3\pi/4 < \theta < -\pi/4$.

Note that the entropy has a minimum at $\theta = \arctan 1/3 \simeq 0.1024\pi$, which is at the valence-bond-solid (VBS) point [43], but that it remains a continuous curve. The extremum of the entropy indicates a change in the wave function and can also signal a phase transition even if it remains a continuous curve. Such behavior has also been found in the $1/n$-filled SU(n) $n = 2, 3, 4, 5$ Hubbard model at $U = 0$, where an infinite-order (Kosterlitz-Thouless-like) phase transition takes place [27, 44, 45, 46]. Since there is no sharply defined transition in the entropy, however, additional methods must be used to classify the ground-state properties on either side of an extremum. One possibility is an analysis of the entropy profile $s(\ell)$ as the subsystem size ℓ is changed from $\ell = 0$ to N for fixed model parameters; see below. Note that there is also another minimum in the block entropy at $\theta = -\pi/2$; this corresponds to a point where the model can be partially mapped to the nine-state quantum Potts model whose ground state is exactly known [47, 48]. However, there is no known phase transition at this point.

For models that map to a conformal field theory [49], an analytic expression for the entropy profile has been derived, and this form has been shown to be satisfied by critical spin models. The entropy for a subsystem of length ℓ in a finite system of length N with open boundary conditions within conformal field theory has the form [5]

$$s(\ell) = \frac{c}{6} \ln \left[\frac{2N}{\pi} \sin \left(\frac{\pi \ell}{N} \right) \right] + g \ , \tag{24.8}$$

where c is the central charge. This quantity contains a constant term which depends on the ground-state degeneracy and a constant shift g which depends on the boundary conditions. As will be shown below, there can be an additional oscillatory term which decays with system size and distance from the boundary as a power law [50, 51].

A new method to analyze the oscillatory nature of the finite subsystem entropy $s(\ell)$, is based on the Fourier spectrum of $s(\ell)$,

$$\widetilde{s}(q) = \frac{1}{N} \sum_{\ell=0}^{N} \mathrm{e}^{-\mathrm{i}q\ell} s(\ell) \ , \tag{24.9}$$

with $s(0) = s(N) = 0$, where $q = 2\pi n/N$ and $n = 0, \ldots, N-1$, is appropriate to study cases when no true phase transition takes place, i.e., when only the character of the decaying correlation function changes.

Figure 24.4(a) shows the block entropy at $\theta = \pi/4$ for the so-called trimerized phase, a phase characterized by three soft modes in the energy spectrum at $k = 0, \pm 2\pi/3$ [35, 36, 37]. The solid line is a fit using (24.8), which yields $c = 2$ in agreement with [30, 31, 32] and [52]. The oscillation in the entropy with a period of three is related to these three soft modes, as is apparent in Fig. 24.4(b) in which the peaks in the Fourier spectrum appear at $k = 0, \pm 2\pi/3$ [53]. A similar analysis at $\theta = -\pi/4$ yields $c = 3/2$ in the thermodynamic limit. The corresponding $\widetilde{s}(q)$ has

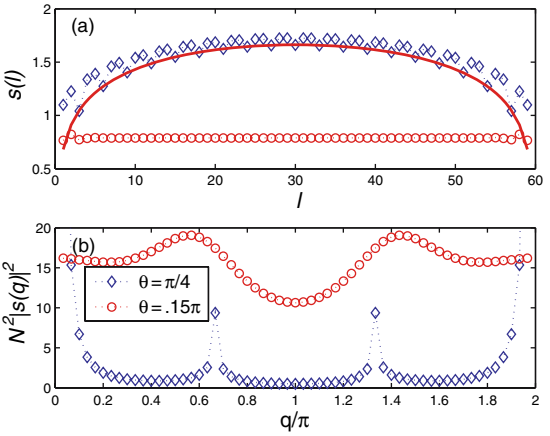

Fig. 24.4. **(a)** Von Neumann entropy of a subsystem of size ℓ on an $L = 60$ bilinear-biquadratic spin chain for $\theta = \pi/4$ and $\theta = 0.15\pi$. The fit to the upper, $\theta = \pi/4$, curve has been carried out using (24.8), and yields $c = 2$, $q^* = 2\pi/3$. The lower curve, for $\theta = 0.15\pi$, has a small value and the entropy saturates because the phase is gapped. **(b)** Power spectrum $N^2|\widetilde{s}(q)|^2$ of the data of **(a)**. The curve for $\theta = 0.15\pi$ has been multiplied by a factor of 5 to enhance its readability on this scale

peaks at $q = 0$ and π for finite systems. It is known that for $\theta < \pi/4$ the soft modes become gapped and the minimum of the energy spectrum moves from $q = 2\pi/3$ toward $q = \pi$ as θ approaches the VBS point [43].

In order to characterize the various phases in the thermodynamic limit, a finite-size extrapolation must be carried out. Fig. 24.5 displays the behavior of $\widetilde{s}(q^*)$ with system size for a number of values of θ that are representative of the different phases. The wave vector q^* is chosen to be appropriate for the corresponding phase, for example, $q^* = 2\pi/3$ in the trimerized phase. The value $q^* = 0.53$ for $\theta = 0.15\pi$ (in the incommensurate phase) is the location of the incommensurate peak; see Fig. 24.4(b). As can be seen, all $\widetilde{s}(q^*) \to 0$ for $N \to \infty$, except in the range $-3\pi/4 < \theta < -\pi/4$ where $\widetilde{s}(q = \pi)$ remains finite, signaling the bond-ordered nature of the dimerized phase. Note that the $q^* = 0$ peak (not shown) also scales to a finite value in much of the phase diagram.

In Fig. 24.6, we summarize the behavior of $\widetilde{s}(q)$ for finite systems and in the $N \to \infty$ limit. We determine the position of the peaks in $\widetilde{s}(q)$ on finite systems by finding the maxima in splines fit through the discrete allowed q points. Infinite-system behavior, obtained from extrapolations (see Fig. 24.5), is also depicted. In the ferromagnetic phase, $\theta < -3\pi/4, \theta > \pi/2$, there is a sole peak at $q^* = 0$, as expected. The $q^* = 0$ peak is present for all θ and persists in the thermodynamic limit. In the dimer phase, $-3\pi/4 < \theta < -\pi/4$, the $q^* = \pi$ peak persists in the thermodynamic limit (see Fig. 24.5). Two different behaviors can be seen in the Haldane phase, $-\pi/4 < \theta < \pi/4$; for $\theta < \theta_{\mathrm{VBS}}$, the $q^* = \pi$ peak present in finite-size systems vanishes in the thermodynamic limit. For $\theta > \theta_{\mathrm{VBS}}$, the incommensurate peak present only in finite systems can be seen to move from $q = 0$ to $2\pi/3$ as θ goes towards $\pi/4$, as also seen in Fig. 24.4. Finally, in the spin nematic phase, $\pi/4 < \theta < \pi/2$, there is a peak at $q^* = 2\pi/3$ which scales to zero as $N \to \infty$.

Therefore, incommensurability can be detected by the entropy analysis as well. It is known [54] that the VBS point is a disorder point, where incommensurate

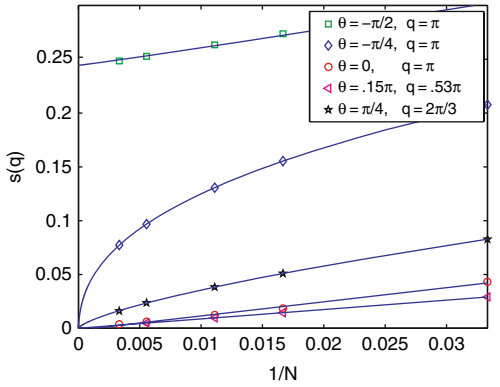

Fig. 24.5. Finite-size scaling of $\widetilde{s}(q)$ for a number of representative values of θ at the appropriate wave vector q. The continuous lines are fits to a form $AN^{-\alpha} + B$

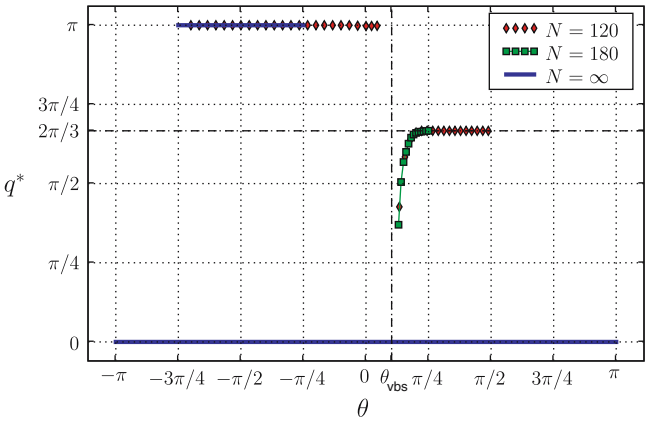

Fig. 24.6. Position of the peak q^* in the Fourier-transformed block entropy $|\widetilde{s}(q)|^2$ plotted as a function of the parameter θ for the bilinear-biquadratic spin chain on system sizes of $N = 120$ and $N = 180$ (for higher resolution near θ_{VBS}), as well as in the thermodynamic limit. The peak at $q^* = 0$ on finite systems, which is present for all θ, has been removed for readability

oscillations appear in the decaying correlation function; however, the shift of the minimum of the static structure factor appears only at a larger value, $\theta_{\mathrm{L}} = 0.138\pi$, the Lifshitz point. In contrast to this, the minimum of the block entropy shown in Fig. 24.3 is exactly at the VBS point, and therefore indicates the location of the commensurate-incommensurate transition correctly.

A similar analysis can be carried out for the frustrated $J - J'$ Heisenberg spin $1/2$ chain with Hamiltonian

$$H = \sum_i \left[J\left(\boldsymbol{S}_i \cdot \boldsymbol{S}_{i+1}\right) + J'\left(\boldsymbol{S}_i \cdot \boldsymbol{S}_{i+2}\right) \right] , \tag{24.10}$$

with the ratio J'/J ($J', J > 0$) playing the role of the parameter θ in the bilinear-biquadratic model. For $J'/J < J_c \approx 0.2411$, the model is in a critical Heisenberg phase, while a spin gap develops for $J'/J > J_c$. At $J'/J = 0.5$, the Majumdar-Ghosh point, the model is exactly solvable and the ground state is a product of

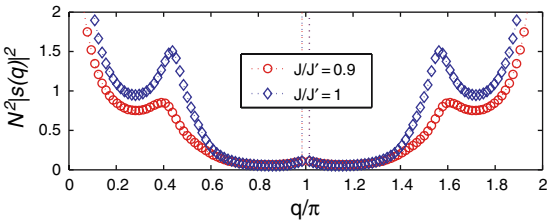

Fig. 24.7. Power spectrum of the block entropy $N^2|\widetilde{s}(q)|^2$ for the frustrated Heisenberg chain at $J/J' = 1$, calculated on a chain of length $N = 128$

local dimers [55]. As a function of J'/J, the block entropy is continuous, but has a minimum at $J/J' = 0.5$. For $J/J' > 0.5$ an extra peak appears in the Fourier spectrum of $\widetilde{s}(q)$ and moves from 0 to $\pi/2$ as J/J' gets larger. The development of the incommensurate peaks near $J/J' = 1$ can be seen in Fig. 24.7.

24.3 Discussion and Outlook

In this chapter, we have sketched the intimate relationship between quantum information and the family of density-matrix renormalization group methods. The fundamental approximation in the DMRG can perhaps be best understood in quantum information terms: The wave function of a bipartite system is most accurately represented by minimizing the quantum information loss, or by carrying out an optimal lossy quantum data compression. The quantum information loss can be used within the DMRG as a measure of the accuracy that is alternate to the discarded weight of density matrix eigenvalues and has a number of advantages. We have outlined some efforts to use quantum information quantities, specifically, the one-site entropy and the mutual quantum information for two sites, to optimize the ordering of single-particle orbitals in non-local Hamiltonians. Finally, we have discussed how the von Neumann entropy calculated during the DMRG procedure can be used to study quantum phase transitions. Jumps, cusps, and minima or maxima in the mid-block entropy signal first, second, and infinite-order phase transitions, while information about the spatial structure of phase can be gleaned from dependence of the entropy on the position of the partition of the bipartite system and from its Fourier transform.

There are a number of possibilities to further apply quantum information theory within the DMRG approach. For example, the possibility of using various quantum information entropies, the entropy reduction by basis-state transformations, entanglement localization, bounds on accessible information of mixed states, and the description of the dynamics of mixed states in terms of an effective temperature have not yet been fully explored [1, 56]. These aspects of quantum information are also closely related to a more quantum-information oriented formulation of the DMRG which has led to more general algorithms based on matrix-product states and their generalizations. Application of these generalizations include systems at finite temperature, systems with dissipation, the calculation of dynamical and time-dependent behavior, and more efficient treatment of higher-dimensional systems [2].

Acknowledgements

This work was supported in part by Hungarian Research Fund (OTKA) Grants No. K 68340 and NF 61726 and by the János Bolyai Research Fund.

References

1. A. Galindo, M. Martin-Delgado, Rev. Mod. Phys. **74**, 347 (2002) 653, 662
2. U. Schollwöck, Rev. Mod. Phys. **77**, 259 (2005) 653, 654, 662
3. G. Vidal, J. Latorre, E. Rico, A. Kitaev, Phys. Rev. Lett. **90**, 227902 (2003) 654
4. J. Latorre, E. Rico, G. Vidal, Quant. Inf. and Comp. **4**, 48 (2004) 654
5. P. Calabrese, J. Cardy, J. Stat. Mech.: Theor. Exp. (2004) 654, 658
6. M. Srednicki, Phys. Rev. Lett. **71**, 666 (1993) 654
7. S. White, Phys. Rev. Lett. **69**, 2863 (1992) 654
8. S. White, Phys. Rev. B **48**, 10345 (1993) 654
9. R. Noack, S. Manmana, in *Lectures on the physics of highly correlated electron systems IX*, *AIP Conference proceedings*, Vol. 789, ed. by A. Avella, F. Mancini (Melville, New York, 2005), *AIP Conference proceedings*, Vol. 789, p. 93 654
10. Ö. Legeza, J. Sólyom, Phys. Rev. B **68**, 195116 (2003) 654, 656
11. O. Legeza, J. Sólyom, Phys. Rev. B **70**, 205118 (2004) 654, 655, 656
12. F. Verstraete, D. Porras, J. Cirac, Phys. Rev. Lett. **93**, 227205 (2004) 654
13. F. Verstraete, J. Cirac. URL `http://arxiv.org/abs/cond-mat/0407066`. Preprint 654
14. S.R. White, A. Feiguin, Phys. Rev. Lett. **93**, 076401 (2004) 654
15. A.J. Daley, C. Kollath, U. Schollwöck, G. Vidal, J. Stat. Mech.: Theor. Exp. P04005 (2004) 654
16. O. Legeza, F. Gebhard, J. Rissler, Phys. Rev. B **74**, 195112 (2006) 654, 656, 657
17. B. Schumacher, Phys. Rev. A **51**, 2738 (1995) 654
18. R. Jozsa, J. Mod. Opt. **41**, 2315 (1994) 654
19. G. Vidal, Phys. Rev. Lett. **91**, 147902 (2003) 654
20. A. Kholevo, Probl. Inf. Transm.(USSR) **177**, 9 (1973) 654
21. C. Fuchs, C. Caves, Phys. Rev. Lett. **73**, 3047 (1994) 654, 655
22. J. Rissler, R. Noack, S. White, Chem. Phys. **323**, 519 (2006) 656, 657
23. T. Xiang, Phys. Rev. B **53**, 10445 (1996) 656
24. S. Nishimoto, E. Jeckelmann, F. Gebhard, R. Noack, Phys. Rev. B **65**, 165114 (2002) 656
25. G.L. Chan, M. Head-Gordon, J. Chem. Phys. **116**, 4462 (2002) 656
26. P. Zanardi, Phys. Rev. A **65**, 42101 (2002) 657
27. S.J. Gu, S.S. Deng, Y.Q. Li, H.Q. Lin, Phys. Rev. Lett. **93**, 86402 (2004) 657, 658
28. J. Vidal, G. Palacios, R. Mosseri, Phys. Rev. A **69**, 022107 (2004) 657
29. J. Vidal, R. Mosseri, J. Dukelsky, Phys. Rev. A **69**, 054101 (2004) 657
30. G. Fath, J. Sólyom, Phys. Rev. B **44**, 11836 (1991) 658, 659
31. G. Fath, J. Sólyom, Phys. Rev. B **47**, 872 (1993) 658, 659
32. G. Fath, J. Sólyom, Phys. Rev. B **51**, 3620 (1995) 658, 659
33. L. Takhtajan, Phys. Lett. A **87**, 479 (1982) 658
34. H.M. Babujian, Phys. Lett. A **90**, 479 (1982) 658
35. G. Uimin, JETP Lett. **12**, 225 (1970) 658, 659
36. C. Lai, J. Math. Phys. **15**, 1675 (1974) 658, 659
37. B. Sutherland, Phys. Rev. B **12**, 3795 (1975) 658, 659
38. A. Chubukov, J. Phys. Condens. Matter **2**, 1593 (1990) 658
39. A. Chubukov, Phys. Rev. B **43**, 3337 (1991) 658
40. A. Läuchli, G. Schmid, S. Trebst, Phys. Rev. B **74**, 144426 (2006) 658
41. K. Buchta, G. Fath, Ö. Legeza, J. Sólyom, Phys. Rev. B **72**, 054433 (2005) 658
42. Ö. Legeza, J. Sólyom, Phys. Rev. Lett. **96**, 116401 (2006) 658
43. I. Affleck, T. Kennedy, E. Lieb, H. Tasaki, Phys. Rev. Lett. **59**, 799 (1987) 658, 660

44. D. Larsson, H. Johannesson, Phys. Rev. Lett. **95**, 196406 (2005) 658
45. D. Larsson, H. Johannesson, Phys. Rev. A **73**, 155108 (2007) 658
46. K. Buchta, Ö. Legeza, E.S.J. Sólyom, Phys. Rev. B **75**, 155108 (2007) 658
47. J. Parkinson, J. Phys. C **20**, L1029 (1987) 658
48. J. Parkinson, J. Phys. C **21**, 3793 (1988) 658
49. C. Holzhey, F. Larsen, F. Wilczek, Nucl. Phys. B **424**, 443 (1994) 658
50. I. Affleck, A.W.W. Ludwig, Phys. Rev. Lett. **67**, 161 (1991) 659
51. N. Laflorencie, E.S. Sørensen, M.S. Chang, I. Affleck, Phys. Rev. Lett. **96**, 100603 (2006) 659
52. C. Itoi, M.H. Kato, Phys. Rev. B **55**, 8295 (1997) 659
53. Ö. Legeza, J. Sólyom, L. Tincani, R.M. Noack, Phys. Rev. Lett. **99**, 087203 (2007) 659
54. U. Schollwöck, T. Jolicoeur, T. Garel, Phys. Rev. B **53**, 3304 (1996) 660
55. C.K. Majumdar, D.K. Ghosh, J. Mat. Phys. **10**, 1388, 1399 (1969) 662
56. L. Amico, R. Fazio, A. Osterloh, V. Vedral. URL `http://arxiv.org/abs/quant-ph/0703044`. Preprint 662